# Effects of $CO_2$ on the structure of silicate melts considering the degree of polymerization under pressure

Shino HAYAFUNE [*,**], Tatsuya SAKAMAKI [*], Haruki ICHIKAWA [*], Yohei ONODERA [**], Shinji KOHARA [**], Ken-ichi FUNAKOSHI [***], and Akio SUZUKI [*]

[*] *Department of Earth Science, Graduate School of Science, Tohoku University, Sendai, 980-8578, Japan*

[**] *Center for Basic Research on Materials, National Institute for Materials Science (NIMS), Ibaraki, 305-0047, Japan*

[***] *Neutron Science and Technology Center, Comprehensive Research Organization for Science and Society (CROSS), Ibaraki, 319-1106, Japan*

Corresponding author:
Name: Shino Hayafune
E-mail address: shino.hayafune.t1@dc.tohoku.ac.jp

## ABSTRACT

Carbon dioxide ($CO_2$) is a prevalent volatile in Earth's interior, but its effects on the structural properties of magmas or silicate melts remain insufficiently understood. Previous studies have indicated that the addition of $CO_2$ can decrease the viscosity of silicate melts, but only if they are fully polymerized. In this study, we explored the effects of $CO_2$ considering the degree of polymerization on the structure of silicate melts at high pressures of up to ~5 GPa using in situ synchrotron X-ray diffraction (XRD) and classical molecular dynamics (MD) simulations. The first sharp diffraction peak (FSDP) position of the X-ray structural factor $S(Q)$, which shows the periodicity of an intermediate-range structure, was not affected by the addition of $CO_2$ for partially depolymerized sodium silicate melt ($Na_2Si_3O_7$). On the other hand, the height of the FSDP for fully polymerized silicate melt ($SiO_2$) slightly decreased, indicating that the Si–O network structure was disordered by the addition of $CO_2$. This difference in the behavior of the FSDP may be attributed to the type of carbon species.

**Keywords**: silicate melt structure, $CO_2$, carbonate ion, high pressure

## INTRODUCTION

Carbon dioxide ($CO_2$) is an important volatile in Earth's interior. $CO_2$-bearing (i.e., carbonated) magmas such as kimberlite are known to be generated deep in Earth's interior (e.g., Keshav et al., 2005). To uncover the migration behavior of carbonated magma in deep Earth, the transport properties of analogs such as silicate melts have been studied, including density and viscosity. Measurements at high pressures have revealed that the addition of $CO_2$ decreases the density of silicate melts (e.g., Sakamaki et al., 2011). Although measurements of the viscosity are more limited, they indicate that the effect of $CO_2$ on the viscosity is affected by the degree of polymerization of silicate melts. The degree of polymerization is often expressed in terms of the parameter NBO/T, which is defined as the ratio between the number of nonbridging oxygen (NBO) atoms and the number of tetrahedrally coordinated (i.e., network-forming) cations (T) (Mysen and Richet, 2019). Adding $CO_2$ has been shown to decrease the viscosity of fully polymerized silicate melts (i.e., NBO/T = 0). For example, Suzuki (2018) reported that adding 0.5 wt% $CO_2$ reduced the viscosity of molten jadeite ($NaAlSi_2O_6$, NBO/T = 0) by one to two orders of magnitude. In contrast, Brearley and Montana (1989) reported that adding 0.5 wt% $CO_2$ had no effect on the viscosity of molten sodium melilite ($NaCaAlSi_2O_7$), which is partially depolymerized (NBO/T = 0.67) under the assumption that Al is entirely tetrahedrally coordinated. The physical properties of magmas are known to be sensitive to the atomic structure (e.g., Sakamaki, 2018). Thus, understanding the effects of $CO_2$ on the structures of silicate melts at high pressures and temperatures is important for clarifying the migration behavior of carbonated magmas.

In this study, we conducted in situ X-ray diffraction (XRD) measurements complemented by molecular dynamics (MD) simulations to investigate the effects of $CO_2$ on the structure of a sodium silicate melt ($Na_2Si_3O_7$, NBO/T = 0.67) at high pressures. MD simulations were further conducted to investigate the effects of $CO_2$ on the structures of silicate melts considering the degree of polymerization.

## METHODS

### Experiment

Dry $Na_2Si_3O_7$ was prepared in powder form from reagent-grade $SiO_2$ and $Na_2SiO_3$, and carbonated $Na_2Si_3O_7$ (0.5 wt% $CO_2$) was prepared in powder form by adding $Na_2CO_3$ as the $CO_2$ source. The amount of $CO_2$ was kept below the solubility of $Na_2Si_3O_7$ melt under the experimental conditions to avoid the liquid immiscibility of the silicate and carbonate melts (Dasgupta et al., 2006; Brooker and Kjarsgaard, 2011). Figure 1 shows a cross section of the high-pressure cell assembly for the experiment. A boron–epoxy cube was used as a pressure-transmitting medium, and the pressure marker was a mixture of MgO and *h*–BN (3:2 weight ratio). The temperature *T* was estimated by calibration against the electric power (Fig. S1), which was performed in a preliminary experiment using a cell assembly with a $W_{97}Re_3$–$W_{75}Re_{25}$ thermocouple (Fig. S2). The pressure *P* was calculated using the third-order Birch–Murnaghan equations of state of MgO (Tange et al., 2009). XRD measurements were conducted in situ using MAX80 (Shimomura, 1984), which is a cubic multi-anvil apparatus installed at the AR-NE5C beamline of the Photon Factory Advanced Ring (PF-AR) in Tsukuba, Japan. Measurements were conducted over a *P* range of 2–5 GPa, and *T* was kept at just above the melting point of the silicates. White X-rays in the energy range of 20–140 keV were used as incident X-rays, and scattered X-rays from the melt were detected with a germanium detector. The detailed experimental procedure is summarized in Ohashi et al. (2018).

We derived two different functions to analyze the structure of the silicate melts. The total structure factor $S(Q)$ was determined by correcting diffraction profiles using the MCEDX code (Funakoshi, 1997), and it is defined as

$$S(Q) = \frac{I^{coh}(Q)/N - \left[\sum_i \{c_i f_i(Q)\}^2 - \{\sum_i c_i f_i(Q)\}^2\right]}{\{\sum_i c_i f_i(Q)\}^2}, \qquad \text{(Eq. 1)},$$

where $N$, $I^{coh}(Q)$, $c_i$, and $f_i(Q)$ are the number of atoms in the scattering system, coherent scattering intensity, the concentration of atoms *i,* and atomic scattering factor, respectively. The reduced pair distribution function $G(r)$ was used to analyze the local structure and short-range order of the silicate melts, and it is derived as

$$G(r) = \frac{2}{\pi}\int_{Q_{min}}^{Q_{max}} Q\{S(Q) - 1\}M(Q)\sin(Qr)\mathrm{d}Q, \qquad \text{(Eq. 2)},$$

where $r$ is the atomic distance. $M(Q)$ is the Lorch modification function, which was introduced to suppress the termination ripples of $G(r)$ (Lorch, 1969).

## Simulation

Classical MD simulations of dry and carbonated (0.5 and 5.0 wt% $CO_2$) $Na_2Si_3O_7$ and $SiO_2$

melts were performed using the Large-scale Atomic/Molecular Massively Parallel Simulator code (Thompson et al., 2022). The $Na_2Si_3O_7$ melt was partially depolymerized (NBO/T = 0.67), whereas the $SiO_2$ melt was fully polymerized (NBO/T = 0). Table 1 gives the specifications of the simulated systems, where each contained approximately 30,000 particles. We employed the empirical force field developed by Guillot and Sator (2011), which can be used to treat the chemical reaction of $CO_2 + O^{2-} \leftrightarrow CO_3^{2-}$, in which $CO_2$ molecules react with $O^{2-}$ in a silicate melt to form $CO_3^{2-}$ and vice versa. $P$ was kept at 2 or 5 GPa, and $T$ was kept at 2000 K. Ewald summations were applied to evaluate long-range Coulombic interactions. Periodic boundary conditions were imposed in the simulations, and the time step was 1 fs. The simulation was started with atoms assigned random configurations and velocities. We first ran calculations for 50 ps at 2 or 5 GPa and at 3000 K. Then, the systems were cooled to 2000 K for 10 ps and relaxed for 50 ps. All simulations were carried out in the *NPT* (isothermal isobaric) ensemble.

The three-dimensional structure was analyzed to obtain $Q^n$ species (Stebbins, 1995; Mysen and Richet, 2019), carbon species, and ring statistics. The primitive $(Si–O)_n$ ring size distributions for melts were calculated using the SOVA package (Shiga et al., 2023).

## RESULTS AND DISCUSSION

Figure 2 shows the total structure factors $S(Q)$ and reduced pair distribution functions $G(r)$ for dry and carbonated (0.5 wt% $CO_2$) $Na_2Si_3O_7$ melts at high pressures, obtained by XRD measurements. In previous studies, the first sharp diffraction peak (FSDP) of $S(Q)$ for silicate melts has been assigned to a succession of $SiO_4$ polyhedra with corner-sharing oxygen atoms manifested by the periodicity given by $2\pi/Q_{FSDP}$ (Funamori, 2004; Shuseki et al., 2024, Onodera et al., 2019a). Figure 3 shows $S(Q)$ for dry and carbonated (5.0 wt% $CO_2$) $Na_2Si_3O_7$ and $SiO_2$ melts at high pressures, obtained by MD simulations. For the $Na_2Si_3O_7$ melt, the overall features of $S(Q)$ and the FSDP obtained by XRD measurements (Fig. 2a) and MD simulations (Fig. 3a) changed negligibly with the addition of 0.5 wt% $CO_2$. Neither did the overall features of $G(r)$ change significantly (Fig. 2b). Note that as carbon capsules were used as sample containers, there is some concern as to whether $CO_2$ is fully retained during the XRD experiments. The MD simulations confirmed that $S(Q)$ remained the same for both melts with the addition of only 0.5 wt% $CO_2$ (Fig. S3). However, a different behavior was observed when 5.0 wt% $CO_2$ was added to the $SiO_2$ melt, which resulted in a slight decrease in the height of the FSDP (Fig. 3b), indicating that the Si–O network structure became disordered. Slight pressure-dependent changes in $S(Q)$ and $G(r)$ are observed, which are discussed in more detail in the supplementary (see Figs. S4 and S5).

It is also revealed that the degree of polymerization of these melts changed negligibly with the addition of $CO_2$. Figure 4 shows the distributions of $Q^n$ species for dry and carbonated (5.0 wt% $CO_2$) $Na_2Si_3O_7$ and $SiO_2$ melts obtained by MD simulations. It is found that some of the oxygen atoms (several mol%) of $Q^4$ $SiO_4$ tetrahedra occupy the center of the $OSi_3$ triclusters (Fig. S6). The distributions of $Q^n$ species for these melts are almost identical between $CO_2$-free and $CO_2$-bearing conditions, indicating that the degree of polymerization of these melts is almost unchanged. This result is consistent with that reported by Morizet et al. (2015), who used first-principles MD simulations of basaltic melts containing $CO_2$, and showed that $CO_2$ may have a limited effect on the degree of polymerization of basaltic melt. Therefore, a slight decrease in the height of the FSDP observed in $CO_2$-bearing $SiO_2$ melts (Fig. 3b) may not be caused by a change in the degree of polymerization of the melt structure.

Figure 5 shows the fractions of carbon species in the $Na_2Si_3O_7$ and $SiO_2$ melts at 5 GPa, obtained by MD simulations. The pressure dependence of $CO_2/(CO_2+CO_3^{2-})$ for $CO_2$-bearing melts is summarized in Fig. S7. The MD simulations confirmed the formation of two types of carbon species: $CO_2$ and carbonate ions ($CO_3^{2-}$). Previous investigations of carbonated quenched glasses by infrared (IR) spectroscopy (Mysen, 1976; Fine and Stolper, 1986) have revealed that $CO_3^{2-}$ is dominant in depolymerized (basic and ultrabasic) melts, but the depolymerized melt in our study (i.e., $Na_2Si_3O_7$) contained approximately 20% $CO_2$ (Fig. 5a). This discrepancy may be because the previous studies using IR spectroscopy underestimated the abundance of $CO_2$ species of the glasses because the following reaction occurs upon quenching: $CO_2 + O^{2-} \rightarrow CO_3^{2-}$ (Morizet et al., 2001; Guillot and Sator, 2011; Konschak and Keppler, 2014; Vuilleumier et al., 2015). In our MD simulations, we found three types of $CO_3^{2-}$: isolated carbonate ions that were not connected to Si ($CO_3^{2-}$, Fig. 6a), nonbridging carbonate ions connected to one Si atom ($Si–CO_3^{2-}$, Fig. 6b), and network carbonate ions connected to two Si atoms ($Si–CO_3^{2-}–Si$, Fig. 6c). We recognized two structural types of network carbonate ions that connect to two Si atoms in $SiO_2$ melt (Fig. 6c), but it was difficult to qualify their fraction using our program code. The charge neutrality of nonbridging and network carbonate ions in $SiO_2$ melt should be carefully considered. In general, these carbonate ions are considered to interact with network modifier cations such as $Na^+$ and $Ca^+$ (Guillot and Sator, 2011; Ni and Keppler, 2013). Although $SiO_2$ melt does not have such network modifier cations, a considerable amount of carbonate ions exists, probably owing to a structure in the melt where a local charge compensation is not maintained. Indeed, in addition to the bridging oxygen and $Q^4$, we find the presence of $OSi_3$ triclusters (Fig. S6) and $Q^3$ (Fig. 4b) which is the signature of a structure in which a charge compensation is not maintained locally.

The behaviors of FSDP upon the addition of $CO_2$ can be explained by the carbon species in the melts. For $Na_2Si_3O_7$ melt, molecular $CO_2$ and nonbridging carbonate ions predominantly exist (Fig. 5a). Previous results suggest that molecular $CO_2$ is only loosely associated with the melt structure (Ni and Keppler, 2013), and nonbridging carbonate ions are mainly formed by displacement from NBO atoms (Guillot and Sator, 2011). A similar behavior is observed in the FSDP of $\underline{S}(Q)$ where carbonate ions do not greatly change the intermediate-range structure of melt (Figs. 2a, 3a). On the other hand, $SiO_2$ melt has molecular $CO_2$ and carbonate ions as nonbridging and network carbonate ions (Fig. 5b). The Si–O network of the $SiO_2$ melt has a relatively ordered structure in which $SiO_4$ tetrahedra are fully bonded via bridging oxygen atoms. However, the inclusion of nonbridging and network carbonate ions disrupts the order of this network, which causes the reduction in the correlation estimated by the FSDP full width at half maximum (FWHM) (Onodera et al., 2019a) associated with the height decrease of the FSDP (Fig. 3b).

To obtain deep insight into the intermediate-range structure, the $(Si–O)_n$ ring size distribution between dry and $CO_2$-bearing melts is compared. The primitive $(Si–O)_n$ ring size distributions for dry and carbonated (5.0 wt% $CO_2$) $Na_2Si_3O_7$ and $SiO_2$ melts are plotted in Fig. 7. It is found that there is little difference between dry and carbonated melts for $Na_2Si_3O_7$ melt, but a distinct difference was observed for $SiO_2$ melt. As can be seen in Fig. 7b, the large $(Si–O)_n$ rings are transformed into smaller $(Si–O)_n$ rings by nonbridging and network carbonate ions; this is associated with bond interchange under high *P*-*T* conditions. This behavior is different from that caused by alkali ions (network modifier cations) in silicate glass at ambient pressure (Onodera et al., 2019b).

Our results suggest that the addition of $CO_2$ changes the network structure of the fully polymerized $SiO_2$ melt (NBO/T = 0) to some extent, whereas it negligibly changes the network structure of the depolymerized $Na_2Si_3O_7$ melt (NBO/T = 0.67). This behavior can be explained by the structural effect of carbonate species on the network structure of melts.

## ACKNOWLEDGMENTS

We thank K. Obata for assistance with the experimental preparations. This research was performed with the support of JSPS KAKENHI Grant Numbers 20H05878, 20H05881, JP21K18641, and JP23K22588. Synchrotron experiments were conducted at the AR-NE5C beamline with the approval of the High Energy Accelerator Research Organization (KEK) (Proposal Nos. 2021G512 and 2023G519), and the calculations in this study were performed using the Numerical Materials Simulator at the National Institute for Materials Science (NIMS).

## REFERENCES


Brearley M. and Montana A. (1989) The effect of $CO_2$ on the viscosity of silicate liquids at high pressure. *Geochim. Cosmochim. Acta* **53**, 2609–2616.

Brooker R. A. and Kjarsgaard B. A. (2011) Silicate–Carbonate Liquid Immiscibility and Phase Relations in the System $SiO_2$–$Na_2O$–$Al_2O_3$–CaO–$CO_2$ at 0.1–2.5 GPa with Applications to Carbonatite Genesis. *J. Petrol.* **52**, 1281–1305.

Dasgupta R., Hirschmann M. M. and Stalker K. (2006) Immiscible Transition from Carbonate-rich to Silicate-rich Melts in the 3 GPa Melting Interval of Eclogite + $CO_2$ and Genesis of Silica-undersaturated Ocean Island Lavas. *J. Petrol.* **47**, 647–671.

Fine G. and Stolper E. (1986) Dissolved carbon dioxide in basaltic glasses: concentrations and speciation. *Earth Planet. Sci. Lett.* **76**, 263–278.

Funakoshi K. (1997) Energy-dispersive x-ray diffraction study for alkali silicate melts using synchrotron radiation under high pressure and temperature. Ph. D. thesis, Tokyo Institute of Technology.

Funamori N. (2004) Exploratory studies of silicate melt structure at high pressures and temperatures by in situ X-ray diffraction. *J. Geophys. Res.* **109**, B03203.

Ghosh S., Ohtani E., Litasov K., Suzuki A. and Sakamaki T. (2007) Stability of carbonated magmas at the base of the Earth's upper mantle. *Geophys. Res. Lett.* **34**, L22312.

Guillot B. and Sator N. (2011) Carbon dioxide in silicate melts: A molecular dynamics simulation study. *Geochim. Cosmochim. Acta* **75**, 1829–1857.

Keshav S., Corgne A., Gudfinnsson G. H., Bizimis M., McDonough W. F. and Fei Y. (2005) Kimberlite petrogenesis: Insights from clinopyroxene-melt partitioning experiments at 6 GPa in the CaO–MgO–$Al_2O_3$–$SiO_2$–$CO_2$ system. *Geochim. Cosmochim. Acta* **69**, 2829–2845.

Konschak A. and Keppler H. (2014) The speciation of carbon dioxide in silicate melts. *Contrib. Mineral. Petrol.* **167**, 998.

Lorch E. (1969) Neutron diffraction by germania, silica and radiation-damaged silica glasses. *J. Phys. C Solid State Phys.* **2**, 229–237.

Morizet Y., Kohn S. C. and Brooker R. A. (2001) Annealing experiments on $CO_2$-bearing jadeite glass: an insight into the true temperature dependence of $CO_2$ speciation in silicate melts. *Mineral. Mag.* **65**, 701–707.

Morizet Y., Vuilleumier R. and Paris M. (2015) A NMR and molecular dynamics study of $CO_2$-bearing basaltic melts and glasses. *Chem. Geol.* **418**, 89–103.

Mysen B. O. (1976) The role of volatiles in silicate melts: Solubility of carbon dioxide and water in feldspar, pyroxene, and feldspathoid melts to 30 kb and 1625 °C. *Am. J. Sci.* **276**, 969–996.

Mysen B. and Richet P. (2019) Structure and Property Concepts. In *Silicate Glasses and Melts (Second Edition)* Elsevier Science, Amsterdam. pp. 109–141.

Ni H. and Keppler H. (2013) Carbon in Silicate Melts. *Rev. Mineral. Geochem.* **75**, 251–287.

Ohashi T., Sakamaki T., Funakoshi K. and Suzuki A. (2018) Pressure–induced structural changes of basaltic glass. *J. Mineral. Petrol. Sci.* **113**, 286–292.

Onodera Y., Kohara S., Tahara S., Masuno A., Inoue H., Shiga M., Hirata A., Tsuchiya K., Hiraoka Y., Obayashi I., Ohara K., Mizuno A. and Sakata O. (2019a) Understanding diffraction patterns of glassy, liquid and amorphous materials via persistent homology analyses. *J. Ceram. Soc. Jpn.* **127**, 853–863.

Onodera Y., Takimoto Y., Hijiya H., Taniguchi T., Urata S., Inaba S., Fujita S., Obayashi I., Hiraoka Y. and Kohara S. (2019b) Origin of the mixed alkali effect in silicate glass. *NPG Asia Mater.* **11**, 75.

Sakamaki T. (2018) Structure and Properties of Silicate Magmas. In *Magmas Under Pressure: Advances in High-Pressure Experiments on Structure and Properties of Melts* (eds. Y. Kono and C. Sanloup). Elsevier, Amsterdam. pp. 323–341.

Sakamaki T., Ohtani E., Urakawa S., Terasaki H. and Katayama Y. (2011) Density of carbonated peridotite magma at high pressure using an X-ray absorption method. *Am. Mineral.* **96**, 553–557.

Shiga M., Hirata A., Onodera Y. and Masai H. (2023) Ring-originated anisotropy of local structural ordering in amorphous and crystalline silicon dioxide. *Commun. Mater.* **4**, 91.

Shimomura O. (1984) Multi-anvil type X-ray apparatus for synchrotron radiation. *Mater. Res. Soc. Symp. Proceesdings* **22**, 17–20.

Shuseki Y., Kohara S., Kaneko T., Sodeyama K., Onodera Y., Koyama C., Masuno A., Sasaki

S., Hatano S., Shiga M., Obayashi I., Hiraoka Y., Okada J. T., Mizuno A., Watanabe Y., Nakata Y., Ohara K., Murakami M., Tucker M. G., McDonnell M. T., Oda H. and Ishikawa T. (2024) Atomic and Electronic Structure in MgO–$SiO_2$. *J. Phys. Chem. A* **128**, 716–726.

Stebbins J. F. ed. (1995) Dynamics and structure of silicate and oxide melts: Nuclear Magnetic Resonance studies. In *Reviews in Mineralogy* Mineralogical Society of America, Geochemical Society, Washington. pp. 190–246.

Suzuki A. (2018) Effect of carbon dioxide on the viscosity of a melt of jadeite composition at high pressure. *J. Mineral. Petrol. Sci.* **113**, 47–50.

Tange Y., Nishihara Y. and Tsuchiya T. (2009) Unified analyses for *P*-*V*-*T* equation of state of MgO: A solution for pressure-scale problems in high *P*-*T* experiments. *J. Geophys. Res.* **114**, B03208.

Thompson A. P., Aktulga H. M., Berger R., Bolintineanu D. S., Brown W. M., Crozier P. S., In ’T Veld P. J., Kohlmeyer A., Moore S. G., Nguyen T. D., Shan R., Stevens M. J., Tranchida J., Trott C. and Plimpton S. J. (2022) LAMMPS - a flexible simulation tool for particle-based materials modeling at the atomic, meso, and continuum scales. *Comput. Phys. Commun.* **271**, 108171.

Vuilleumier R., Seitsonen A. P., Sator N. and Guillot B. (2015) Carbon dioxide in silicate melts at upper mantle conditions: Insights from atomistic simulations. *Chem. Geol.* **418**, 77–88.

## TABLE CAPTION

**Table 1**. Number of atoms *i* ($N_i$) of each species in the simulated systems of silicate melts.

## FIGURE CAPTIONS

**Figure 1.** Schematic illustration for the high-*P* cell assemblies used in XRD measurements.

**Figure 2.** Total structure factors $S(Q)$ and reduced pair distribution functions $G(r)$ for dry and carbonated (0.5 wt% $CO_2$) $Na_2Si_3O_7$ melts at high pressures obtained by XRD measurements. Successive curves are displaced upward by 1 (left) and 5 (right) for clarity,

respectively.

**Figure 3.** Total structure factors $S(Q)$ for dry and carbonated (5.0 wt% $CO_2$) melts at high pressures obtained by MD simulations: (a) $Na_2Si_3O_7$ and (b) $SiO_2$. Successive curves are displaced upward by 1 for clarity.

**Figure 4.** Distributions of $Q^n$ species for dry and carbonated (5.0 wt% $CO_2$) melts obtained by MD simulations at 5 GPa and 2000 K: (a) $Na_2Si_3O_7$ and (b) $SiO_2$.

**Figure 5.** Fractions of carbon species in carbonated (5.0 wt% $CO_2$) melts at 5 GPa and 2000 K: (a) $Na_2Si_3O_7$ and (b) $SiO_2$.

**Figure 6.** Characterization of carbonate ions in the silicate melts (snapshots) under high pressure. For clarity, only bonds between atoms are shown. (a) Free carbonate ion, (b) Nonbridging carbonate ion, and (c) Network carbonate ions.

**Figure 7.** Primitive ring size statistics for dry and carbonated (5.0 wt% $CO_2$) (a) $Na_2Si_3O_7$ and (b) $SiO_2$ melts at high pressures obtained by MD simulations.

**Figure S1.** Temperature calibration for the electric power.

**Figure S2.** Schematic illustration for the high-*P* cell assemblies with a thermocouple.

**Figure S3.** Total structure factors $S(Q)$ for dry and carbonated (0.5 wt% $CO_2$) $Na_2Si_3O_7$ melts at high pressures obtained by MD simulations. Successive curves are displaced upward by 1 for clarity.

**Figure S4.** FSDP position for $Na_2Si_3O_7$ melt at high pressures obtained by XRD measurements at 1350 K and MD simulations at 2000 K.

**Figure S5.** Partial pair-correlation functions $g_{SiSi}(r)$ for $Na_2Si_3O_7$ melt at high pressures and 2000 K obtained by MD simulations.

**Figure S6.** Typical atomic configuration formed by the combination of $SiO_4$ tetrahedron and $OSi_3$ tricluster.**Figure S7.** Pressure dependence of $CO_2/(CO_2+CO_3^{2-})$ for carbonated (5.0 wt% $CO_2$) $SiO_2$ and $Na_2Si_3O_7$ melts obtained by MD simulations at 2000 K.

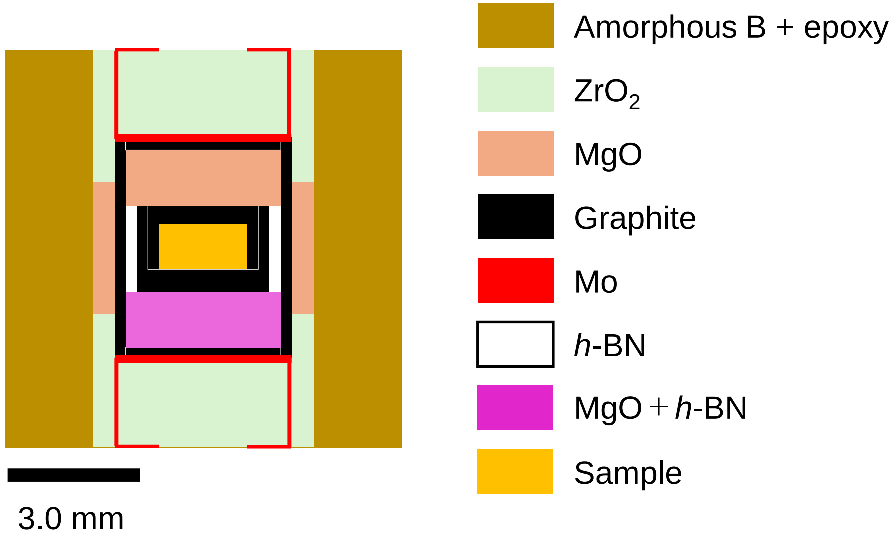


**Figure 1.** Schematic illustration for the high-*P* cell assemblies used in XRD measurements. (S. Hayafune)

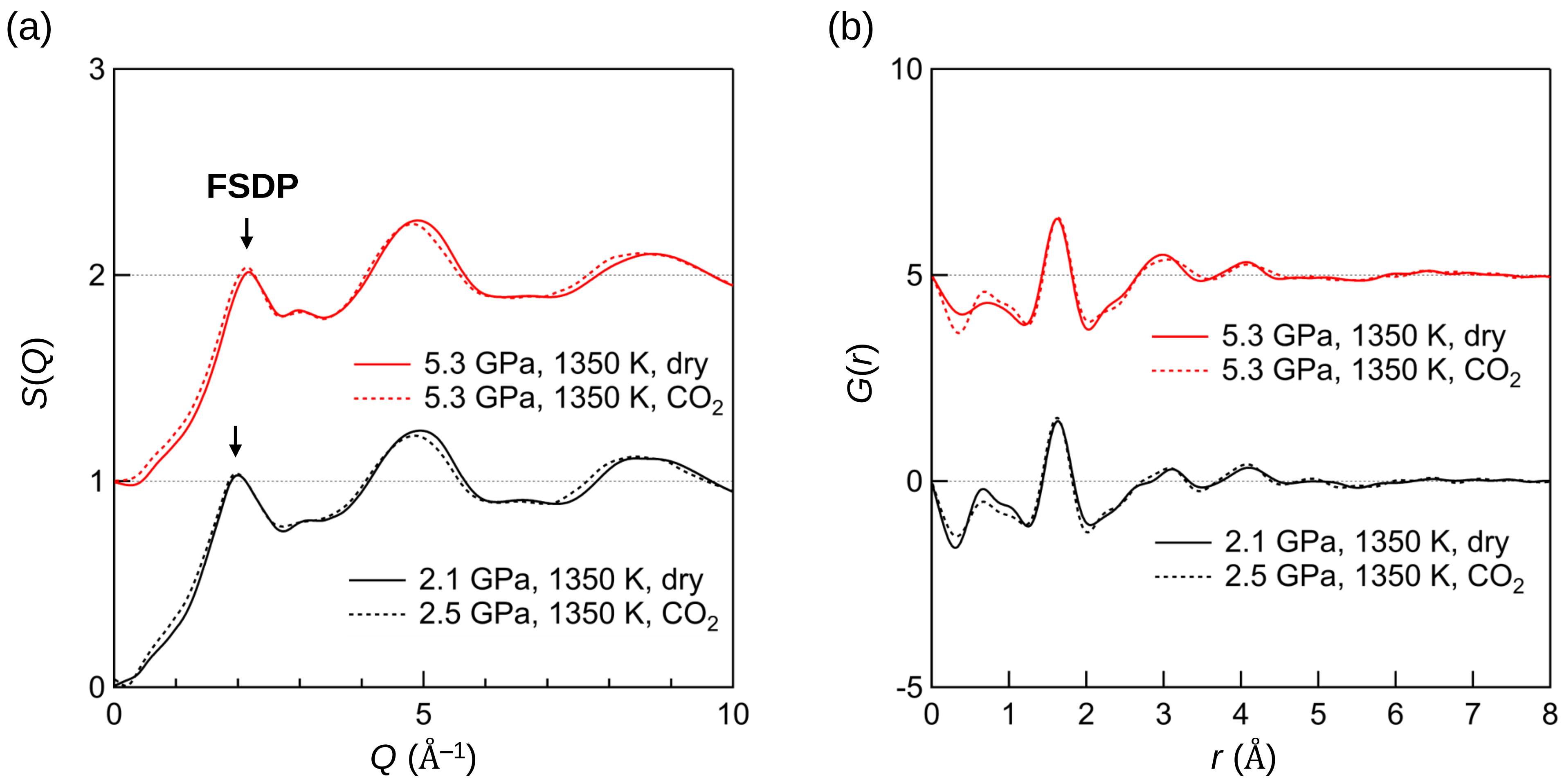


**Figure 2.** Total structure factors $S(Q)$ and reduced pair distribution functions $G(r)$ for dry and carbonated (0.5 wt% $CO_2$) $Na_2Si_3O_7$ melts at high pressures obtained by XRD measurements. Successive curves are displaced upward by 1 (left) and 5 (right) for clarity, respectively. (S.Hayafune)

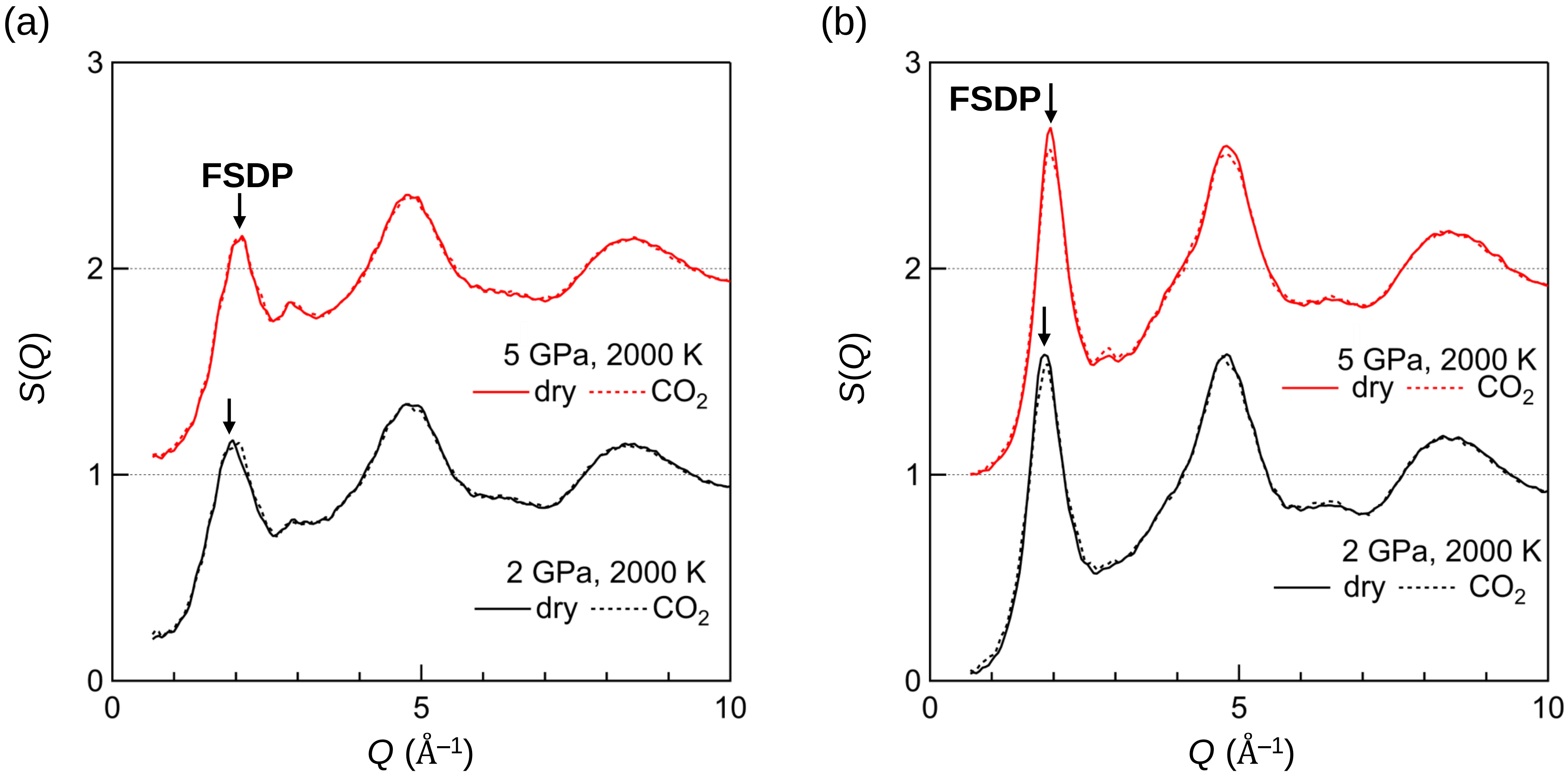


**Figure 3.** Total structure factors $S(Q)$ for dry and carbonated (5.0 wt% $CO_2$) melts at high pressures obtained by MD simulations: (a) $Na_2Si_3O_7$ and (b) $SiO_2$. Successive curves are displaced upward by 1 for clarity. (S. Hayafune)

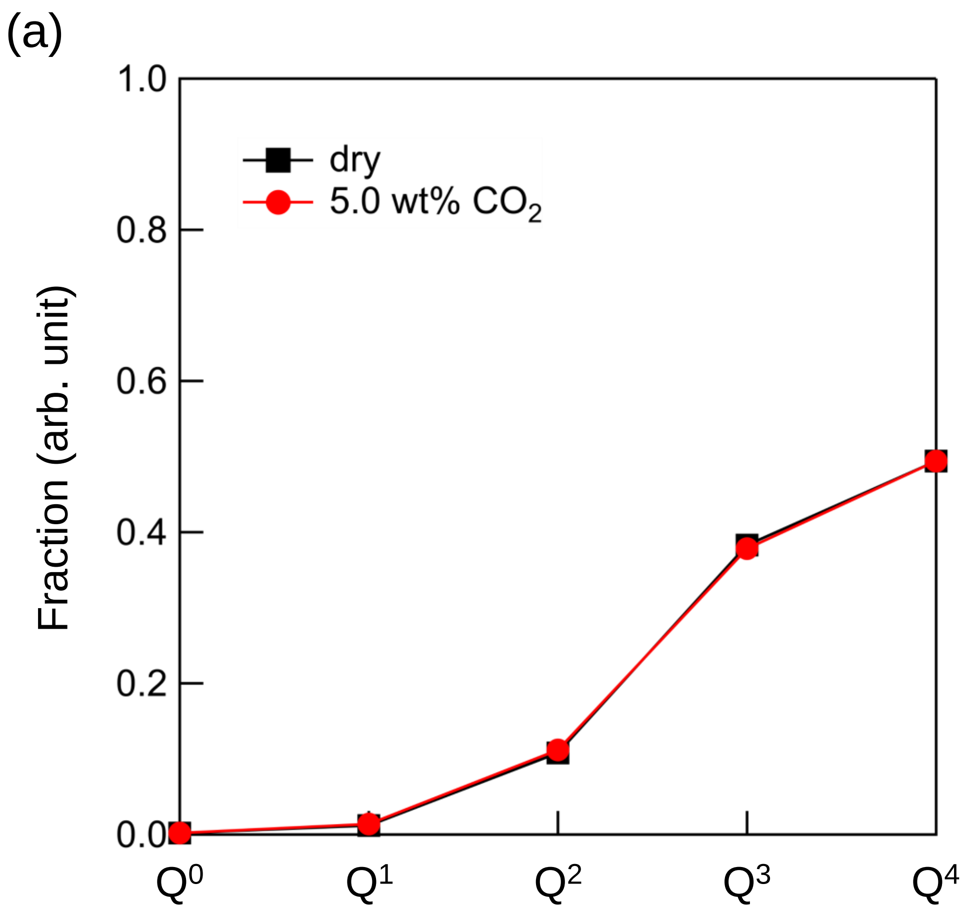


**Figure 4.** Distributions of $Q^n$ species for dry and carbonated (5.0 wt% $CO_2$) melts obtained by MD simulations at 5 GPa and 2000 K : (a) $Na_2Si_3O_7$ and (b) $SiO_2$. (S. Hayafune)

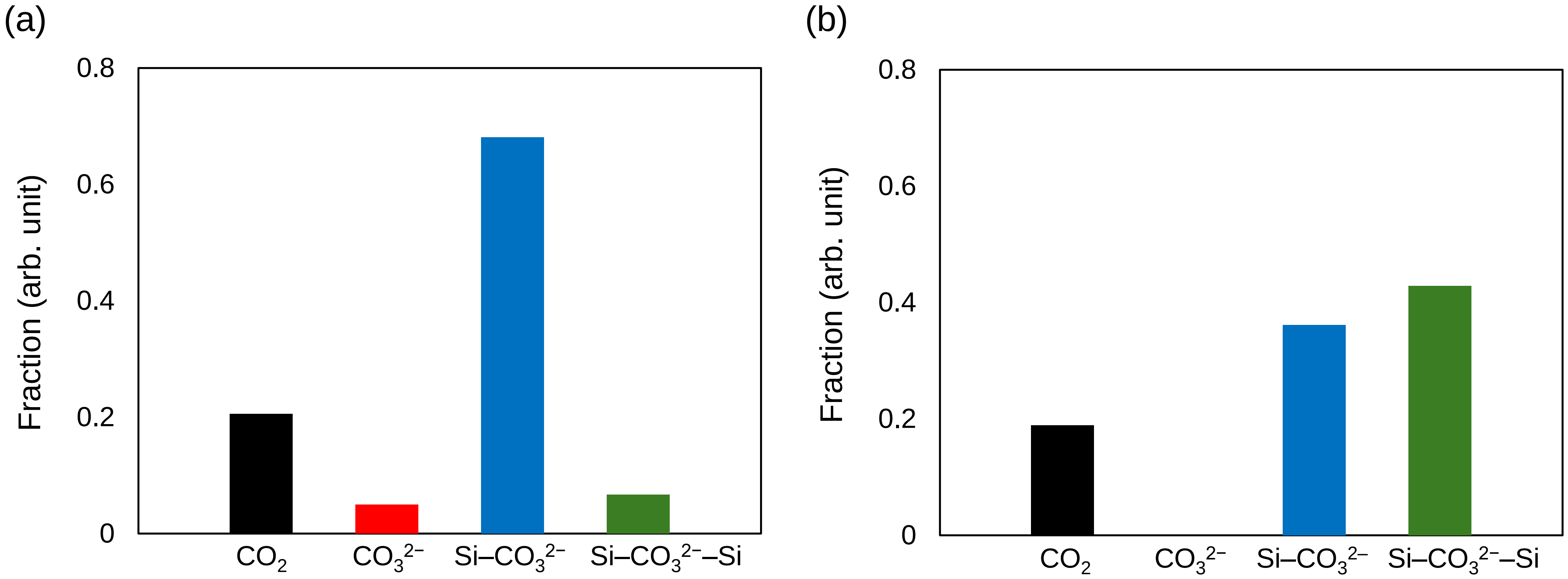


**Figure 5.** Fractions of carbon species in carbonated (5.0 wt% $CO_2$) melts at 5 GPa and 2000 K: (a) $Na_2Si_3O_7$ and (b) $SiO_2$. (S. Hayafune)

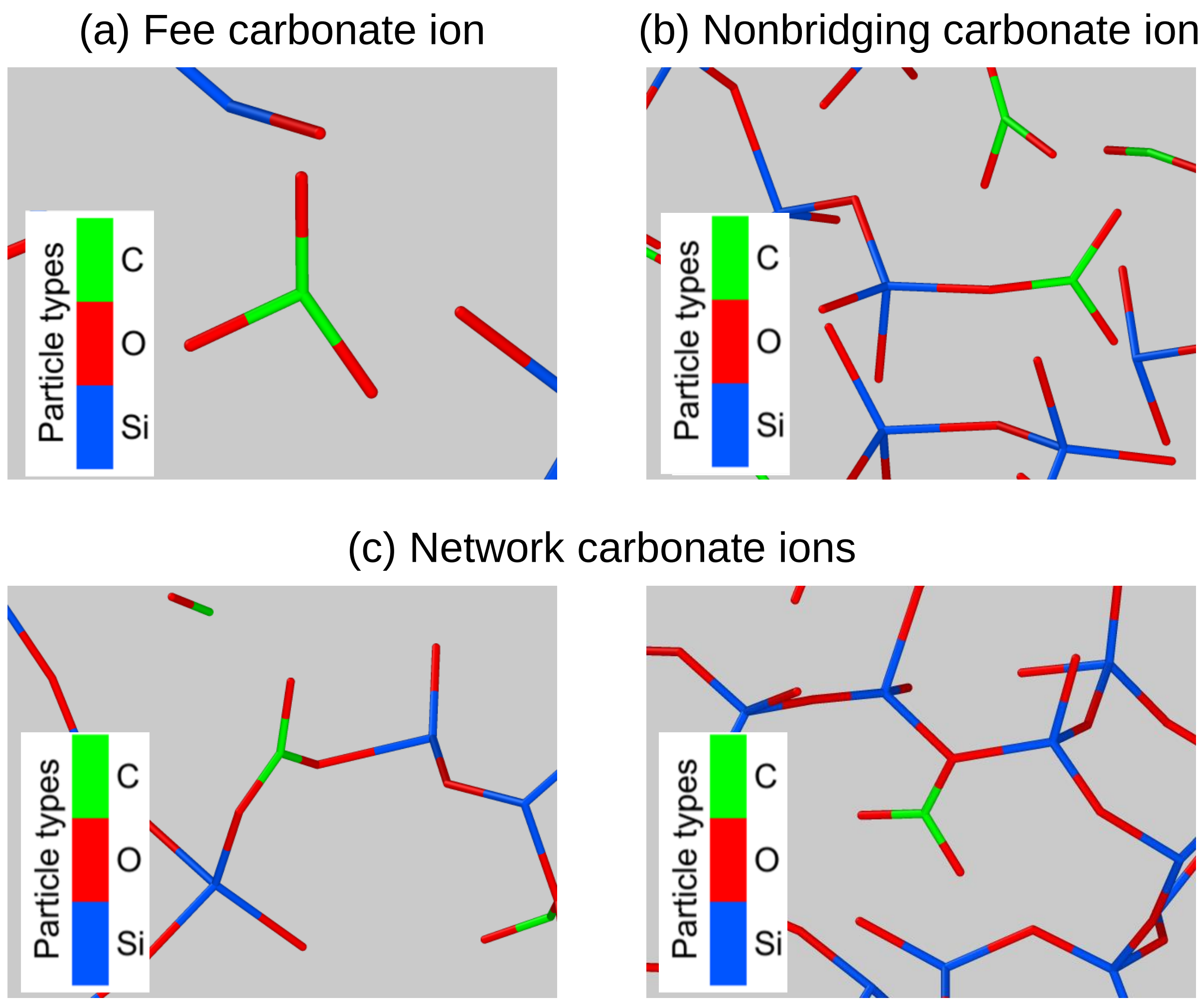


**Figure 6.** Characterization of carbonate ions in the silicate melts (snapshots) under high pressure. For clarity, only bonds between atoms are shown. (a) Free carbonate ion, (b) Nonbridging carbonate ion, and (c) Network carbonate ions. (S. Hayafune)

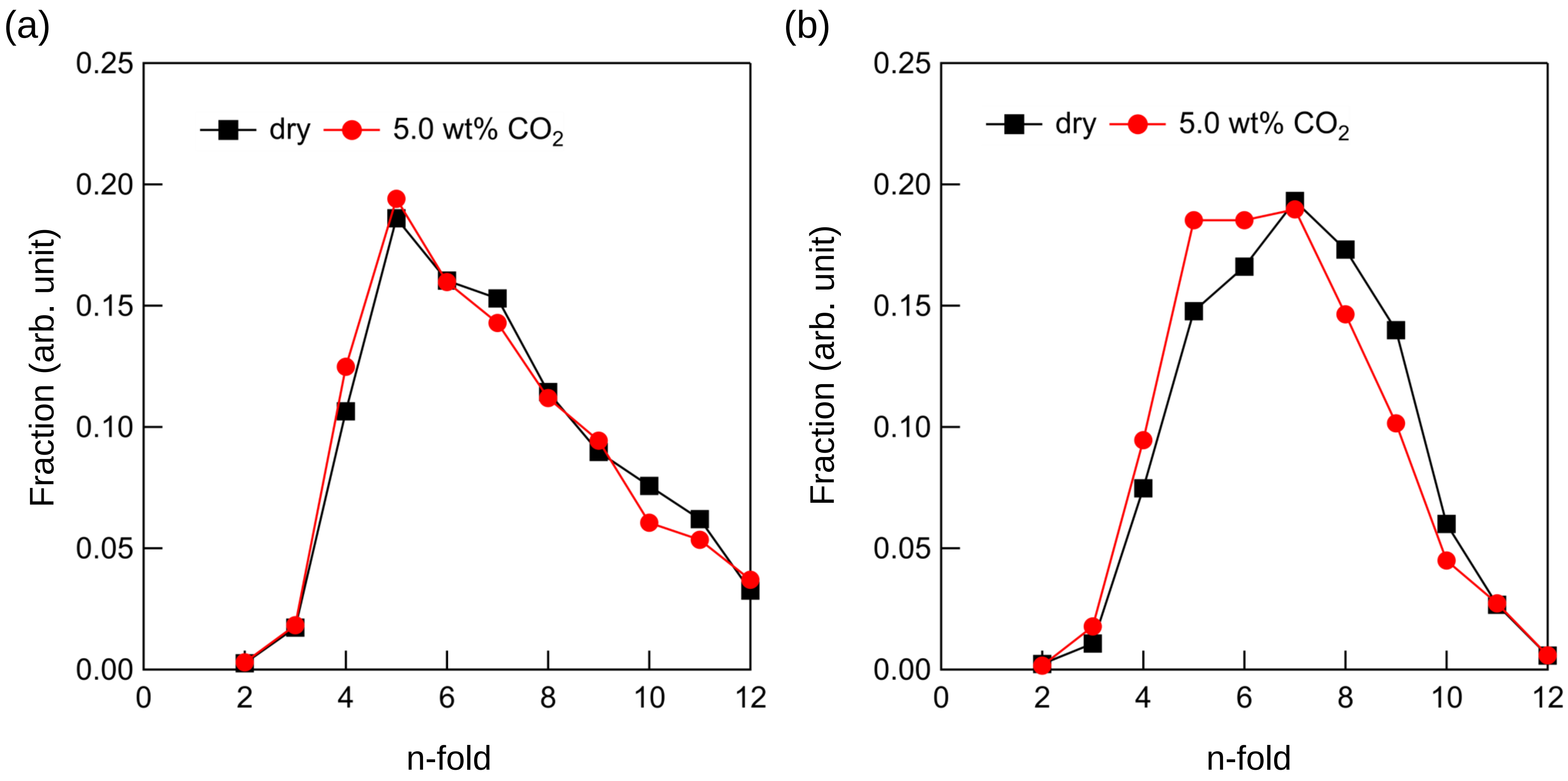


**Figure 7.** Primitive ring size statistics for dry and carbonated (5.0 wt% $CO_2$) (a) $Na_2Si_3O_7$ and (b) $SiO_2$ melts at high pressures obtained by MD simulations. (S. Hayafune)

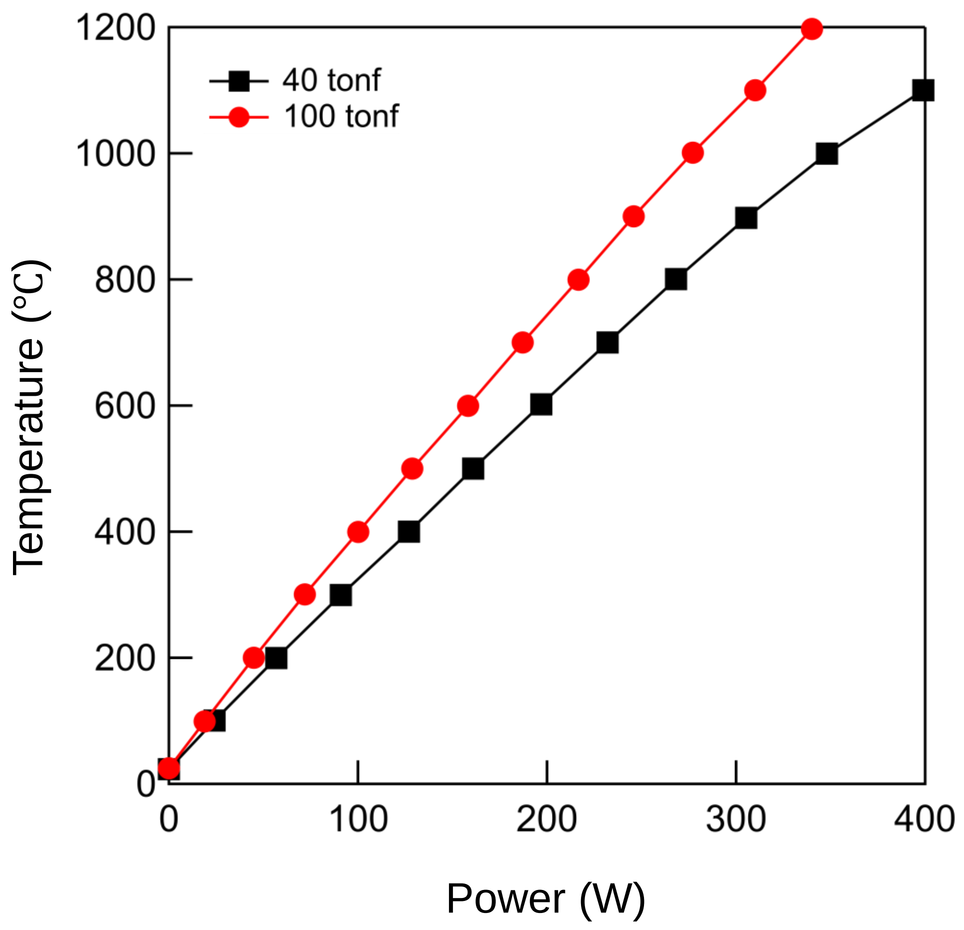


**Figure S1.** Temperature calibration for the electric power.
(S. Hayafune)

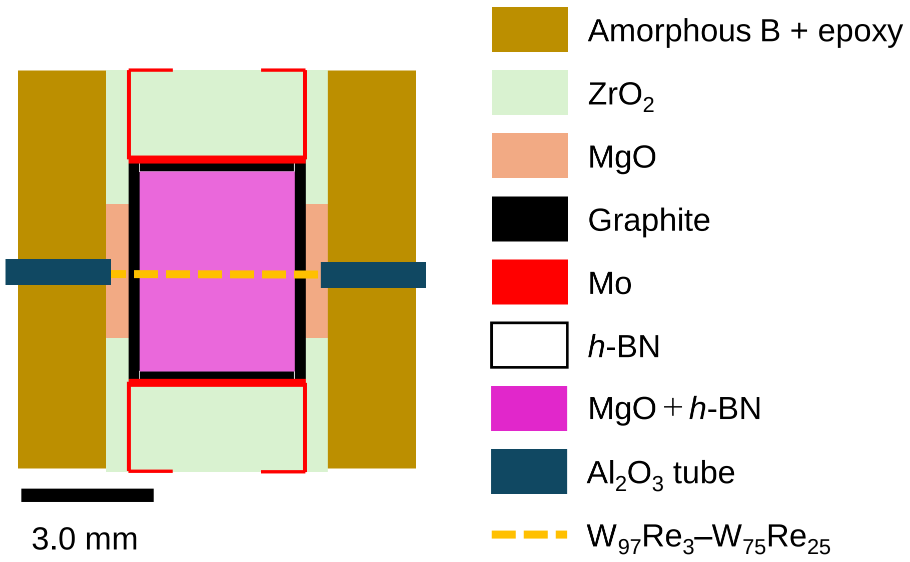


**Figure S2.** Schematic illustration for the high-*P* cell assemblies with a thermocouple. (S. Hayafune)

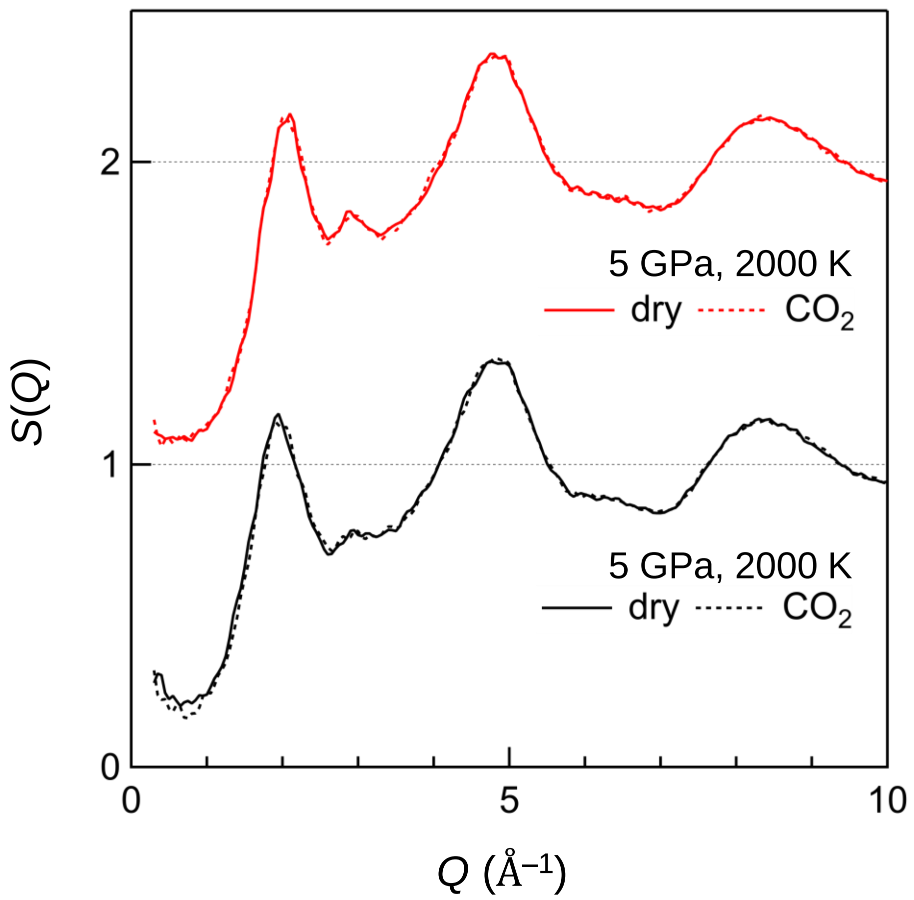


**Figure S3.** Total structure factors $S(Q)$ for dry and carbonated (0.5 wt% $CO_2$) $Na_2Si_3O_7$ melts at high pressures obtained by MD simulations. Successive curves are displaced upward by 1 for clarity. (S. Hayafune)

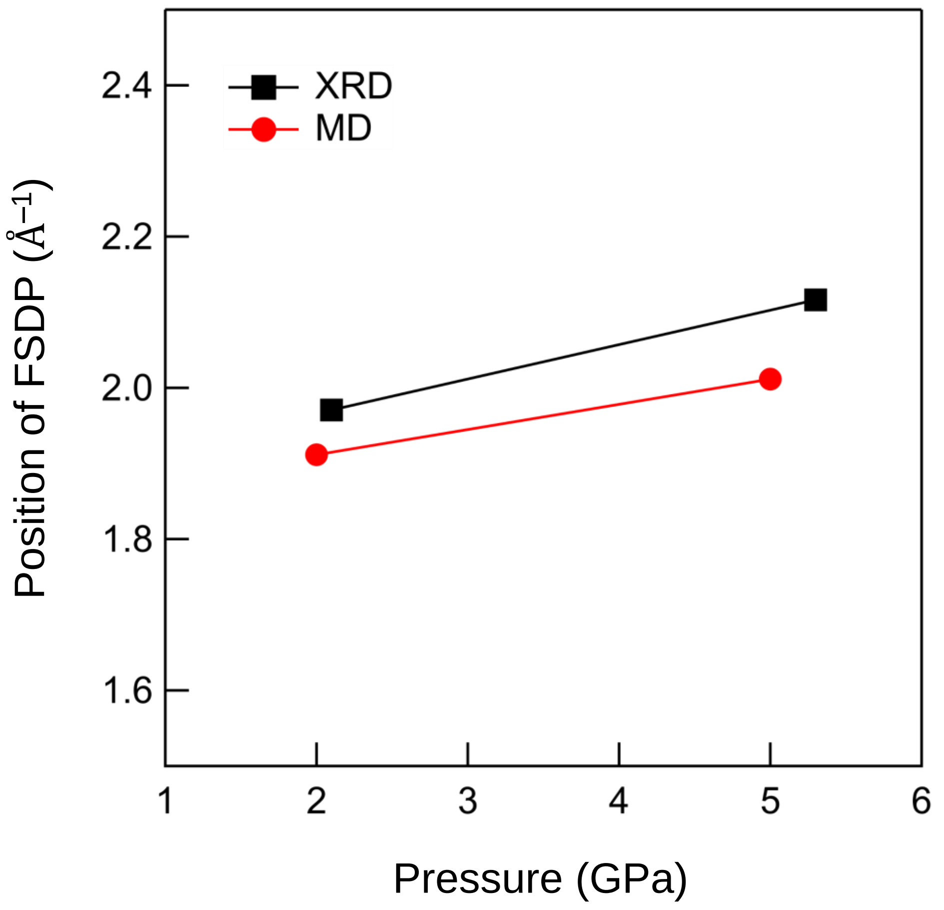


**Figure S4.** FSDP position for $Na_2Si_3O_7$ melt at high pressures obtained by XRD measurements at 1350 K and MD simulations at 2000 K. (S. Hayafune)

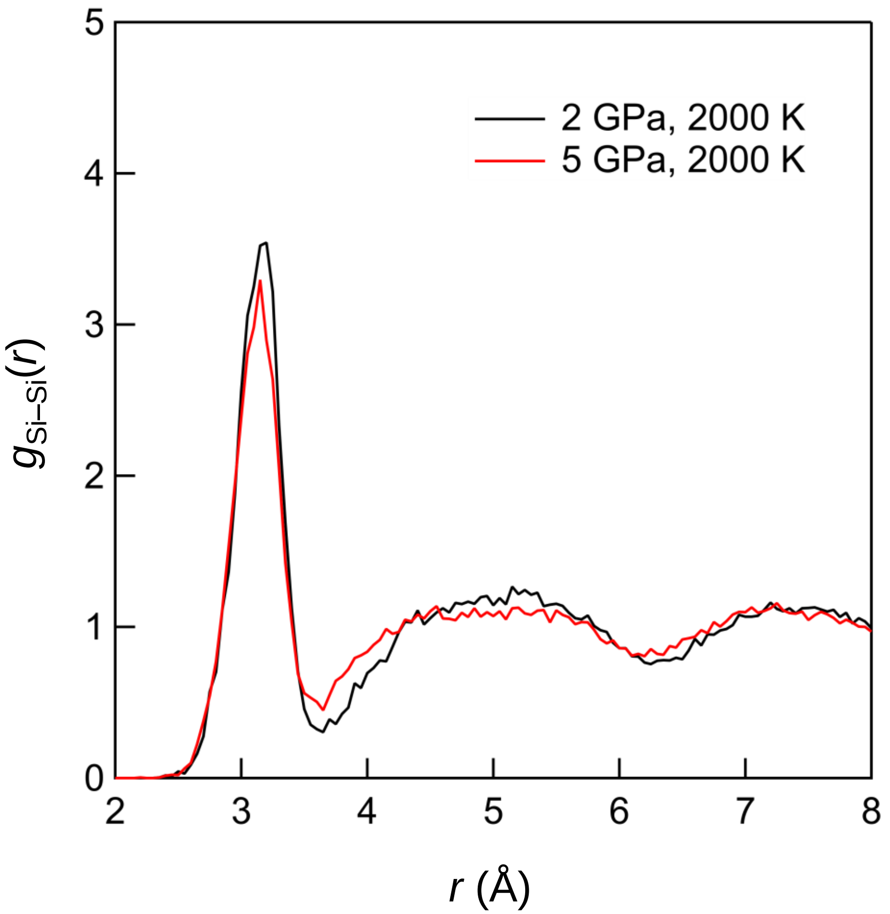


**Figure S5.** Partial pair-correlation functions $g_{SiSi}(r)$ for $Na_2Si_3O_7$ melt at high pressures and 2000 K obtained by MD simulations. (S. Hayafune)

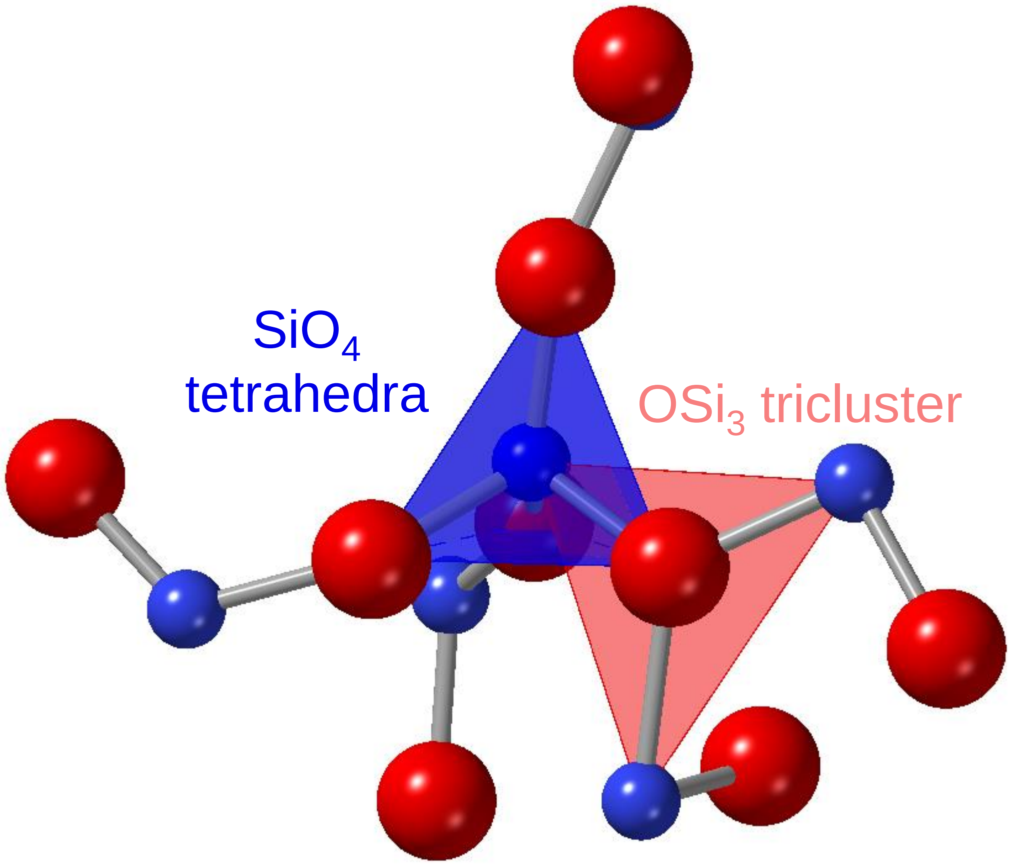


**Figure S6.** Typical atomic configuration formed by the combination of $SiO_4$ tetrahedron and $OSi_3$ tricluster. (S. Hayafune)

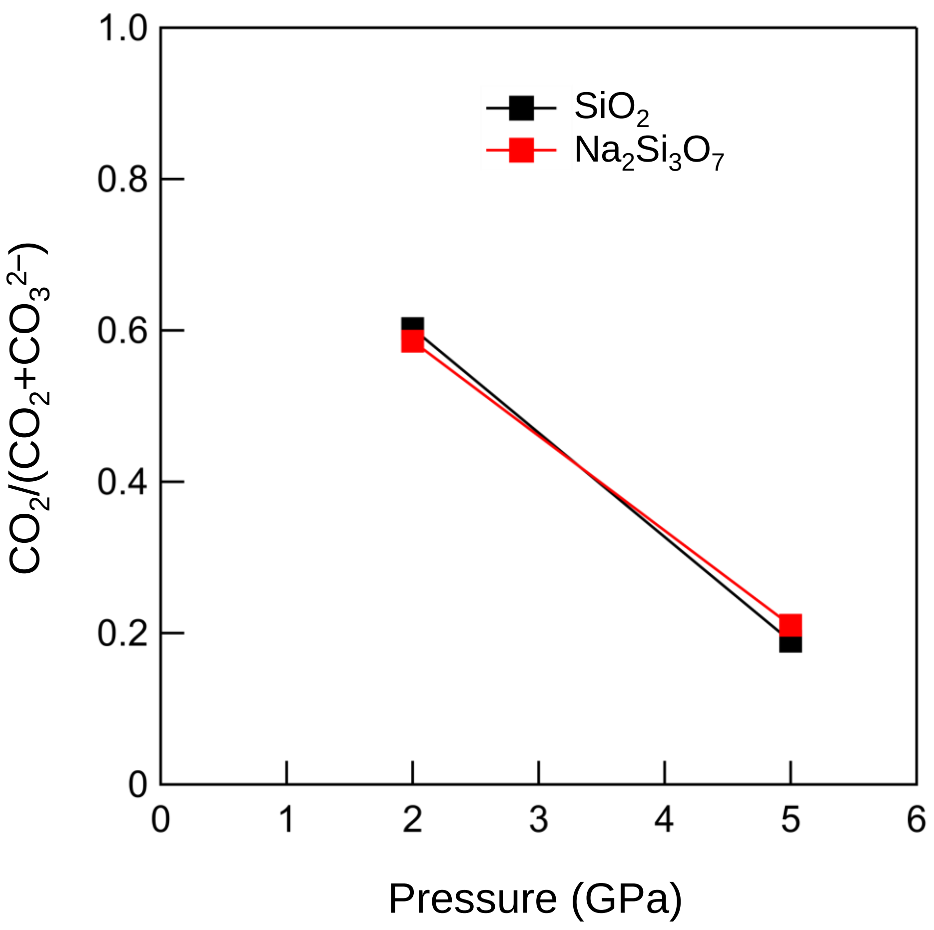


**Figure S7.** Pressure dependence of $CO_2/(CO_2+CO_3^{2-})$ for carbonated (5.0 wt% $CO_2$) $SiO_2$ and $Na_2Si_3O_7$ melts obtained by MD simulations at 2000 K. (S. Hayafune)